Applied Magnetic Resonance (2024) 55:1199–1219
https://doi.org/10.1007/s00723-024-01694-4

Applied
Magnetic Resonance

ORIGINAL PAPER

# EPR Studies of Rare-Earth Manganites $La_{0.7-x}Eu_xSr_{0.3}MnO_3$ ($x = 0.1–0.7$)

**I. Yatsyk[1] · D. V. Mamedov[1] · A. V. Shestakov[2] · I. I. Fazlizhanov[1] · R. M. Eremina[1] · S. I. Andronenko[3] · A. V. Pyataev[3] · S. Vadnala[4] · S. Asthana[5] · S. K. Misra[6]**

Received: 20 March 2024 / Revised: 26 July 2024 / Accepted: 27 July 2024 /
Published online: 6 August 2024


## Abstract

The Europium rare-earth manganites, $La_{0.7-x}Eu_xSr_{0.3}MnO_3$ ($x = 0.0–0.7$), were investigated by the technique of X-band electron paramagnetic resonance (EPR) in the temperature range from 30 to 500 K. As the temperature was lowered, the various samples made transitions from paramagnetic to ferromagnetic phases. Furthermore, coexistence of anywhere from two to three ferromagnetic phases in the various samples was found. The third ferromagnetic phase was observed only in the samples with $x = 0.1$, 0.2, 0.3. The Curie temperatures for the various samples were estimated from the characteristics of the variable-temperature EPR spectra. The EPR data indicated the presence of Griffiths phases in the samples with $x = 0.2$, 0.3, 0.4, 0.5, 0.6, from which the respective Griffiths temperatures were determined. The activation energies were estimated here from the EPR data using the hopping model. The EPR linewidth behavior is found to be consistent with that predicted by the bottlenecked spin-relaxation model. The perovskite $La_{0.5}Eu_{0.2}Sr_{0.3}MnO_3$ is potentially useful in the design of magnetocaloric refrigeration units as a working fluid, since its Curie temperature $T_C$ is found to be close to the room temperature. The various ferromagnetic components in the samples observed here have been resolved only by the technique of EPR, not possible by other techniques.

## 1 Introduction

The manganites have the general formula $A_{1-y}B_yMnO_3$, where A is a rare-earth ion and B = Ca, Ba, Sr. The crystal structure of $La_{1-x}Sr_xMnO_3$ is shown in Fig. 1. They have been extensively studied by the techniques of electron paramagnetic resonance (EPR) and ferromagnetic resonance (FMR) [1–35]. Some of these studies have been focused on understanding the dynamics of spins near and above the ferromagnetic phase transition, the phase separation, manifestation of Jahn–Teller effect and occurrence of Griffiths phase [1–8, 12–14, 19–23]. Their

Extended author information available on the last page of the article

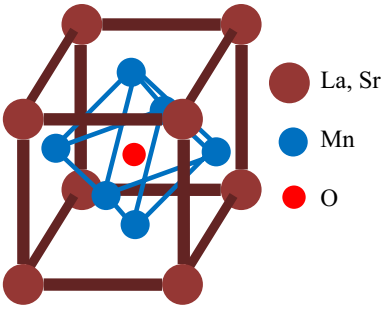


**Fig. 1** Crystal structure of $La_{1-x}Sr_xMnO_3$

transport, magnetic and structural properties depend on the presence of the rare-earth ions ($A^{3+}$), e.g., $La^{3+}$, $Nd^{3+}$, and $Eu^{3+}$, as well as the divalent ions ($B^{2+}$) ions, e.g., $Sr^{2+}$. Recently, Eremina et al. [22] reported studies on phase separation and Griffiths phase in $La_{0.4-x}Eu_{0.6}Sr_xMnO_3$. Investigations of structure, magnetic properties and magnetocaloric effect was carried out by Vadnala et al. [16, 33] on two series of substituted rare-earth manganite compounds:

(1) $Eu^{3+}$-doped compounds $La_{0.7-x}Eu_xSr_{0.3}MnO_3$ ($x=0.0, 0.1, 0.2, 0.3$) [17, 18] and
(2) $Nd^{3+}$-doped compounds $La_{0.7-x}Nd_xSr_{0.3}MnO_3$ ($x=0.0, 0.1, 0.2, 0.3$).

It is known that replacement of the trivalent Lanthanum ion with the divalent Strontium ion in $La_{1-x}Sr_xMnO_3$ compounds leads to a change in their behavior from exhibiting antiferromagnetic exchange to double exchange, achieving the maximum Curie temperature at the Strontium impurity concentration of 30%. Furthermore, the Curie temperature can be changed not only by replacing Lanthanum ions with divalent ions, but also by replacing them with rare-earth ions possessing different spins. The Europium ion contains 6 electrons on the outer shell: $4f^6$, $L=3$, $S=3$, $J=0$. It is expected that the exchange interactions between the rare-earth Europium ions and the iron group Manganese ions are absent and should, therefore, not affect the double exchange that is realized in strontium-doped manganites, in any way. The double-exchange (DE) interaction in the mixed rare-earth manganites $La_{0.7-x}Eu_xSr_{0.3}MnO_3$ is affected by the substitution of the $La^{3+}$ ion by the $Eu^{3+}$ ion. The DE interaction increases when the Mn–O–Mn bond angle decreases due to the substitution of the $La^{3+}$ ion with larger effective radius (1.032 Å) by the $Eu^{3+}$ ion with smaller effective radius (0.95 Å). This decrease in the bond angle becomes larger the greater is the concentration, $x$, of the substituting $Eu^{3+}$ ions. This implies that the DE interaction increases with increasing concentration. In addition, near the phase transitions in manganites, a phase stratification is observed, which manifests itself in the formation of ferromagnetic clusters in the paramagnetic matrix, associated with the formation of Griffiths phase. Using the technique of EPR, one can observe this phase stratification, which manifests itself as splitting into several lines in the EPR spectrum.

### 1.1 Industrial Applications

The strongly correlated manganite oxides studied here have various industrial applications, such as spintronic devices, magnetic refrigeration and infrared devices [36–39]. These materials exhibit colossal magnetoresistance effect in the presence of an external magnetic field. They are useful for development of magnetic data-storage devices [36–38]. Furthermore, at the ferromagnetic to paramagnetic transition temperature, most of the manganites exhibit high temperature coefficient of resistance and large change in magnetic entropy. The high temperature coefficient of resistance (TCR) of manganites is useful for infrared microbolometer detector applications [15, 39], whereas the large change in magnetic entropy with high relative cooling (RC) is useful for magnetic refrigeration [37]. The room temperature transition with high TCR (7.4%) was observed in $Na_{0.5}La_{0.2}Sr_{0.3}MnO_3$:$Ag_2O$ [15] and 3.36% in $La_{0.7-x}Eu_xSr_{0.3}MnO_3$ [17], which are suitable for uncooled microbolometer applications. Similarly, $Na_{0.7-x}La_xSr_{0.3}MnO_3$ [16] compounds, which exhibit a large change in magnetic entropy (~4.78 J/kg × K at 6 Tesla) with high relative cooling (281 J/kg), are suitable for magnetic refrigeration technology.

### 1.2 Motivation for the Present Study

Previous EPR investigations of the Eu-doped $La_{0.7-x}Eu_xSr_{0.3}MnO_3$ ($x = 0.4$, 0.5, 0.6, 0.7) samples [35] did not include the samples with $x = 0.1$, 0.2 and 0.3. Furthermore, they did not carry out measurements at liquid helium and at very high temperatures, which did not lead to an accurate determination of the activation energies. This warrants a more detailed investigation of these compounds. The present paper reports a detailed variable-temperature EPR investigation of Eu-doped manganites $La_{0.7-x}Eu_xSr_{0.3}MnO_3$ ($x = 0.1$, 0.2, 0.3, 0.4, 0.5, 0.6 and 0.7) in the extended temperature range, from 100 to 500 K for the samples with $x = 0.1$, 0.2, 0.3, 0.6 and for the samples with $x = 0.7$, 0.6, 0.5 from 5 to 100 K. The purpose of this paper is to carry out a comprehensive analysis of the ferromagnetic behavior of diluted manganites and the influence of inhomogeneity on their electronic properties from their variable-temperature EPR spectra.

By a detailed analysis of the features of the EPR lines in the paramagnetic region, one can determine the activation energy of the carriers, the temperature of ferromagnetic phase ordering and the Curie–Weiss temperature.

### 1.3 Organization of the Paper

A description of sample preparation is given in Sect. 2. It is followed by the details of EPR measurements and their interpretation for the Perovskites $La_{0.7-x}Eu_xSr_{0.3}MnO_3$ ($x = 0.1$, 0.2, 0.3, 0.4, 0.5, 0.6 and 0.7) in Sect. 2.1. Section 2.2 describes the details of the EPR measurements on $La_{0.7-x}Eu_xSr_{0.3}MnO_3$ ($x = 0.1$–0.7) and the determination of Curie temperatures from the EPR data. The details of Dysonian line shape exhibited by the EPR lines are given in Sect. 2.3. The dependence of

the EPR linewidth on the Eu content in $La_{0.7-x}Eu_xSr_{0.3}MnO_3$ ($x=0.1$–$0.7$) samples is discussed in Sect. 2.4, which also includes estimation of Curie and Curie–Weiss temperatures for these Perovskites. Section 2.4.6 discusses the dependence of Curie temperature on Eu content. Observation of Griffith's phase is presented in Sect. 2.5. Section 2.6 discusses the hopping conductivity and estimation of activation energies for the various samples. The conclusions are summarized in Sect. 3.

## 2 Sample Preparation and EPR Spectra

This section contains details of sample preparation and a discussion of the EPR data obtained on the family of the various rare-earth perovskites $La_{0.7-x}Eu_xSr_{0.3}MnO_3$.

### 2.1 Sample Preparation and Determination of the Ionic State of the Europium Ion in the Manganite Samples

The solid-state reaction route was used to synthesize $La_{0.7-x}Eu_xSr_{0.3}MnO_3$ compounds, where $x=0.0$–$0.7$ in the polycrystalline state, using high purity (more then 99.9%) chemicals $La_2O_3$, $Eu_2O_3$, $SrCO_3Nd_2O_3$ and $Mn_2O_3$ (Sigma Aldrich) as starting materials, mixed in their stoichiometric ratios. The mixtures were ground for 3 h, then calcinated in successive intermediate grinding steps at 1000 °C, 1100 °C and 1200 °C in air for 12 h, subsequently made as pellets and sintered at 1300 °C for 12 h. A "PANanalytic X'pert Pro" was used for X-ray diffraction (XRD) analysis at room temperature. Mossbauer spectroscopy was used to confirm that the ionic state of the Europium ion in the mixed manganites studied here is trivalent, as discussed in "Appendix".

### 2.2 EPR Measurements on $La_{0.7-x}Eu_xSr_{0.3}MnO_3$ ($x=0.1$–$0.7$)

The EPR spectra of the perovskite manganites $La_{0.7-x}Eu_xSr_{0.3}MnO_3$ (LESMO hereafter), where $x=0.1$–$0.7$, were rerecorded on an X-band (9.4 GHz) Bruker EMX/plus spectrometer, equipped with a liquid-nitrogen temperature controller RS 232 in the temperature range of 100–340 K, and a Varian E-12 spectrometer, equipped with a nitrogen gas temperature controller $T_C$ 232, in the temperature range of 300–600 K.

Figure 2 shows the temperature variations of the EPR lines for all the LESMO compounds in the temperature range 100–600 K, for the Eu concentrations $x=0.1$–$0.6$ and from 5 to 340 K for the Eu concentration $x=0.7$. To determine the phase-transition temperatures from the ferromagnetic to the paramagnetic state, the various EPR line shapes were simulated as superpositions of two to four Lorentzian lines (referred to as lines 1, 2, 3, 4 hereafter), depending upon the observed spectrum. The permissible number of lines necessary for a proper description of the spectrum was estimated by the method described in the appendix of the work of Demishev et al. [49]. Each such spectrum was characterized by its own line position, linewidth, and line intensity. Figure 3 shows the decomposition of the experimental

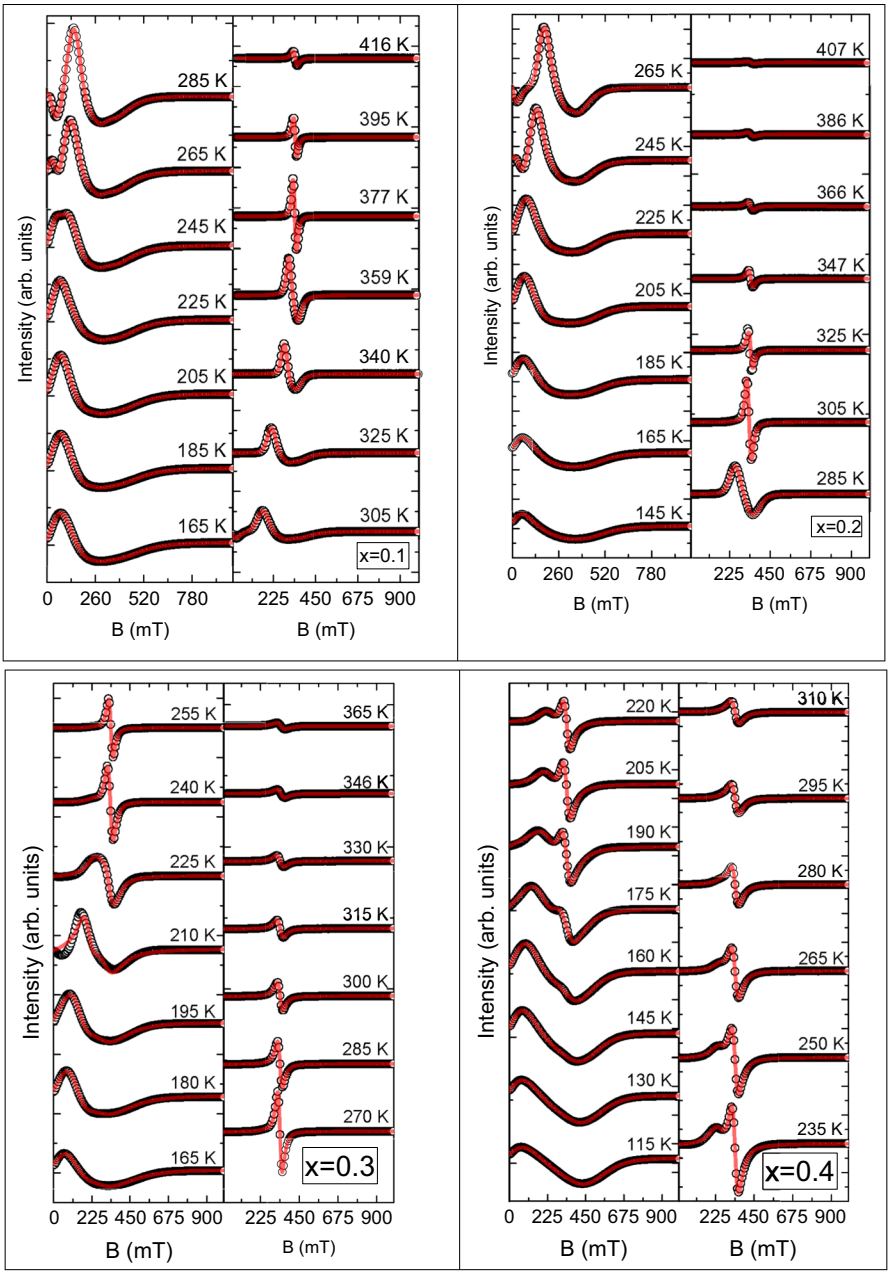


**Fig. 2** Variation of the first derivative EPR spectrum with the change in temperature from 30 to 500 K for the samples $La_{0.7-x}Eu_xSr_{0.3}MnO_3$ ($x = 0.1$–$0.7$). Open symbols are experimental values, solid lines are simulations of the experimental data

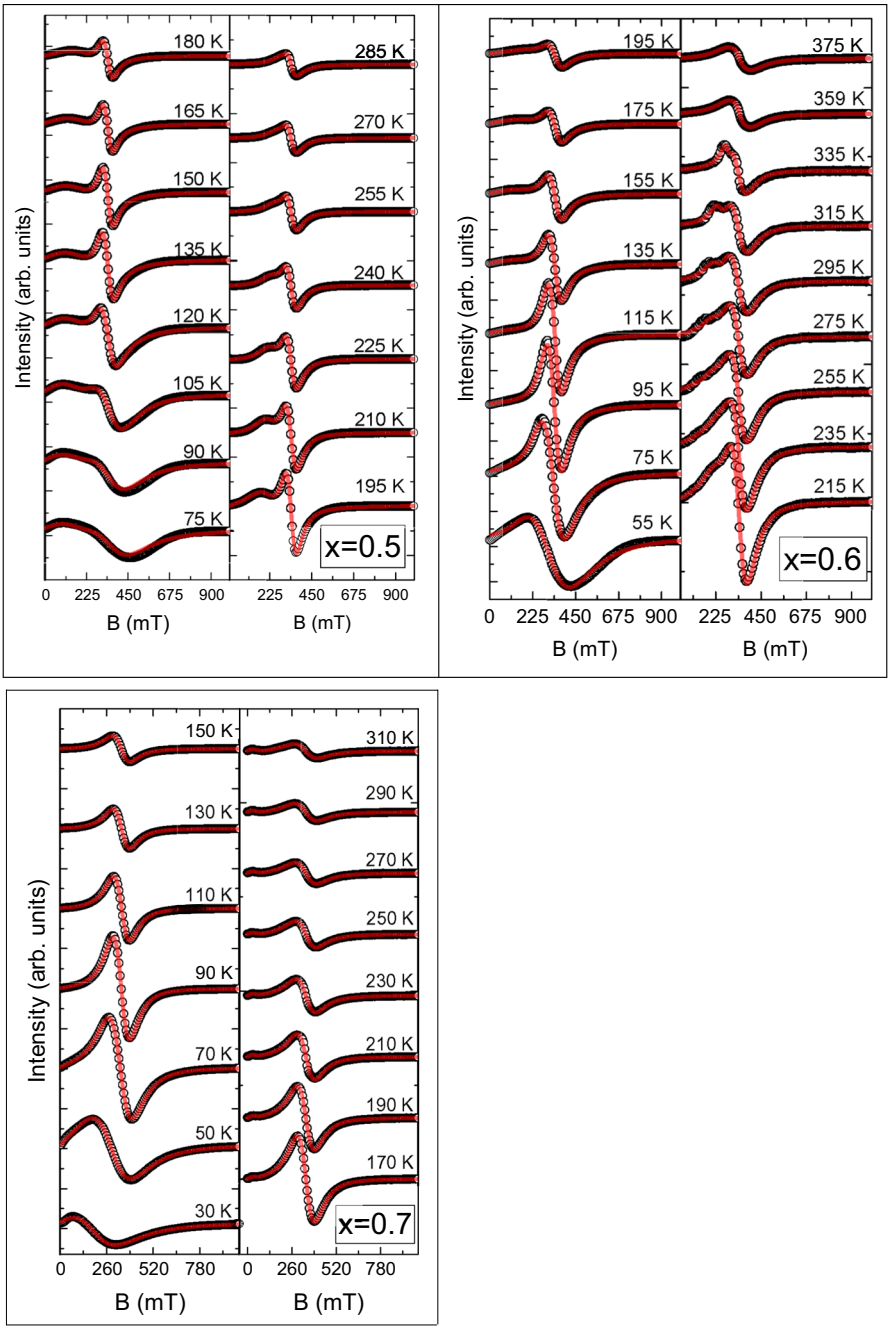


**Fig. 2** (continued)

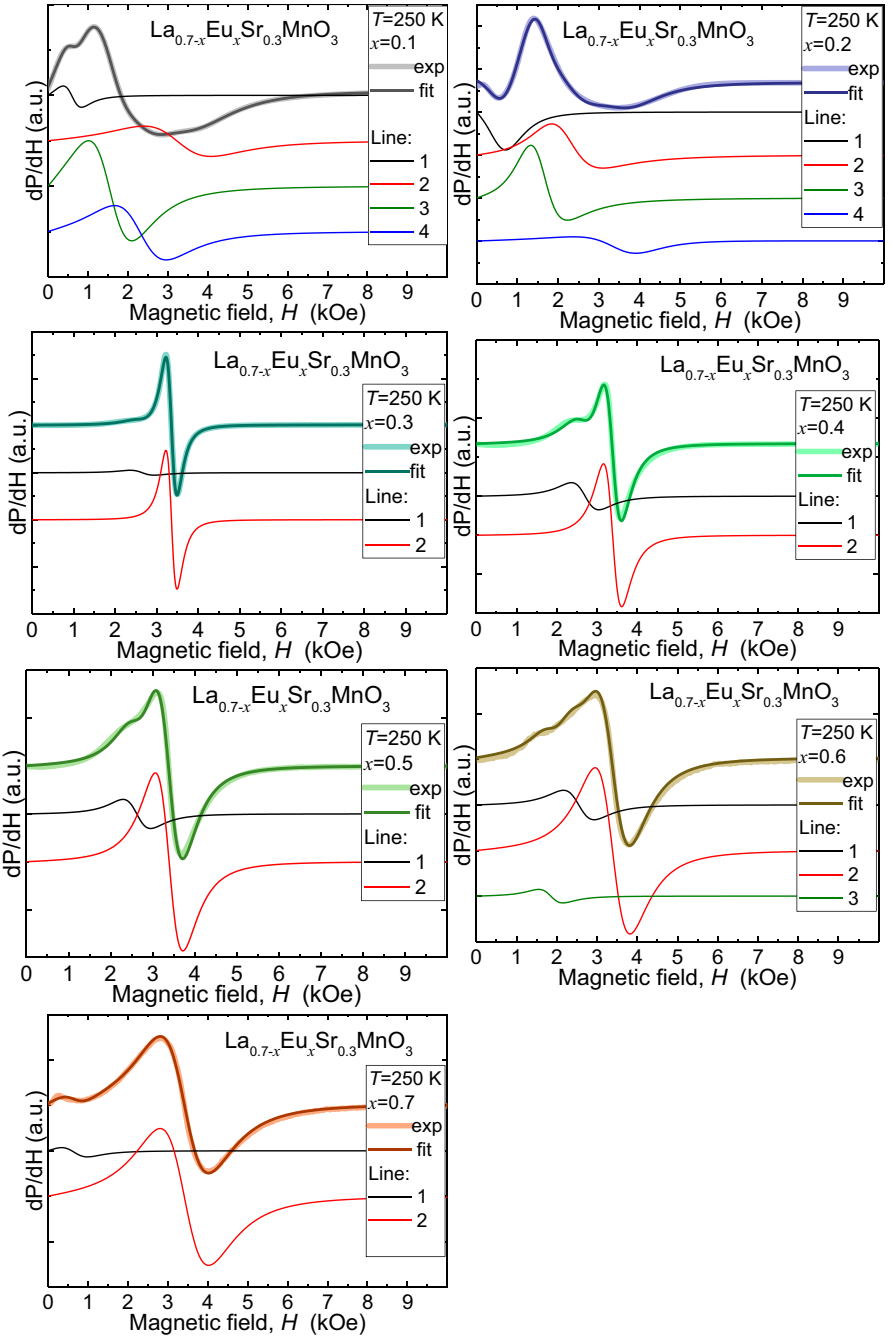


**Fig. 3** Decomposition of the EPR spectra for the samples $La_{0.7-x}Eu_xSr_{0.3}MnO_3$ ($x = 0.1$–$0.7$) into several simulated lines

EPR spectra for the samples $La_{0.7-x}Eu_xSr_{0.3}MnO_3$ ($x=0.1$–$0.7$) at 250 K as superposition of several simulated lines.

### 2.3 Dysonian Line Shape

The first derivative of the line shape $P$ was fitted to the Dysonian line shape [40]:

$$\frac{\partial P}{\partial B} = \frac{\partial}{\partial B}\left[\frac{\Delta B + \alpha(B - B_{res})}{(B - B_{\text{res}})^2 + \Delta B^2} + \frac{\Delta B + \alpha(B + B_{\text{res}})}{(B + B_{\text{res}})^2 + \Delta B^2}\right], \quad (1)$$

where $B_{\text{res}}$ is resonance magnetic field, $\Delta B$ is the linewidth, and $\alpha$ is the asymmetry parameters. Moreover, the value of $|\alpha| \leq 1$, since the samples demonstrate a semiconductor character. The $\alpha$ parameter was zero for the ESR lines for $La_{0.7-x}Eu_xSr_{0.3}MnO_3$ ($x=0.1$; 0.2; 0.3; 0.4; 0.5; 0.6). As for the sample with $x=0.7$, the alpha parameter was zero only for the ESR line at $g=2$.

These overlapped theoretical lines were then fitted to the experimental ones, and the best-fit values of the resonance field, $B_{\text{res}}$, the absorption line width, $\Delta B$, and the intensity $I$ were estimated for each component EPR line of the spectrum. Thus, for each temperature with a step of 5 K, the values of $B_{\text{res}}$, $\Delta B$ and $I$ were estimated (by Eq. 1) for the various component lines, as shown in Fig. 4 for the samples $La_{0.7-x}Eu_xSr_{0.3}MnO_3$ ($x=0.1$, 0.2, 0.3, 0.4, 0.5, 0.6, 0.7).

### 2.4 Estimation of Curie and Curie–Weiss Temperatures for the Perovskites $La_{0.7-x}Eu_xSr_{0.3}MnO_3$ ($x=0.1$–$0.7$)

As seen from Fig. 3, an overlap of several lines is necessary to describe the shape of the spectrum at low temperatures. However, above a certain temperature, only one line is observed in the experimental spectrum, which is the phase-transition temperature from an ordered state to a paramagnetic one. It depends on the relative concentrations of Lanthanum and Europium ions in the samples. When the Lanthanum ion (effective radius 1.032 Å) is increasingly replaced in the A-position in LESMO compounds by the Europium ion (effective radius 0.95 Å), i.e., as the concentration, $x$, of the Europium ion is increased, the ferromagnetic phase transition temperature, $T_C$, was found to decrease, as seen from Table 1. From these plots, the transition temperatures from the ordered ferromagnetic state to the paramagnetic state (Curie temperatures) were estimated for the various samples, as shown in Fig. 5. To this end, the Curie temperature, $T_C$, was determined from the temperature dependence of the derivative of the square of the integrated intensity with respect to temperature integral intensity of $\partial I^2/\partial T$ of line 1 and $T_{C2}$, the ferromagnetic phase transition temperatures for line 2, was estimated from the critical points of these dependencies of line 2, listed in Table 1.

As for the value of $\theta_{CW}$, the Curie–Weiss temperature, it was determined by fitting (Eq. 2) the inverse integrated intensity, $1/I$, to the Curie–Weiss law in the paramagnetic phase:

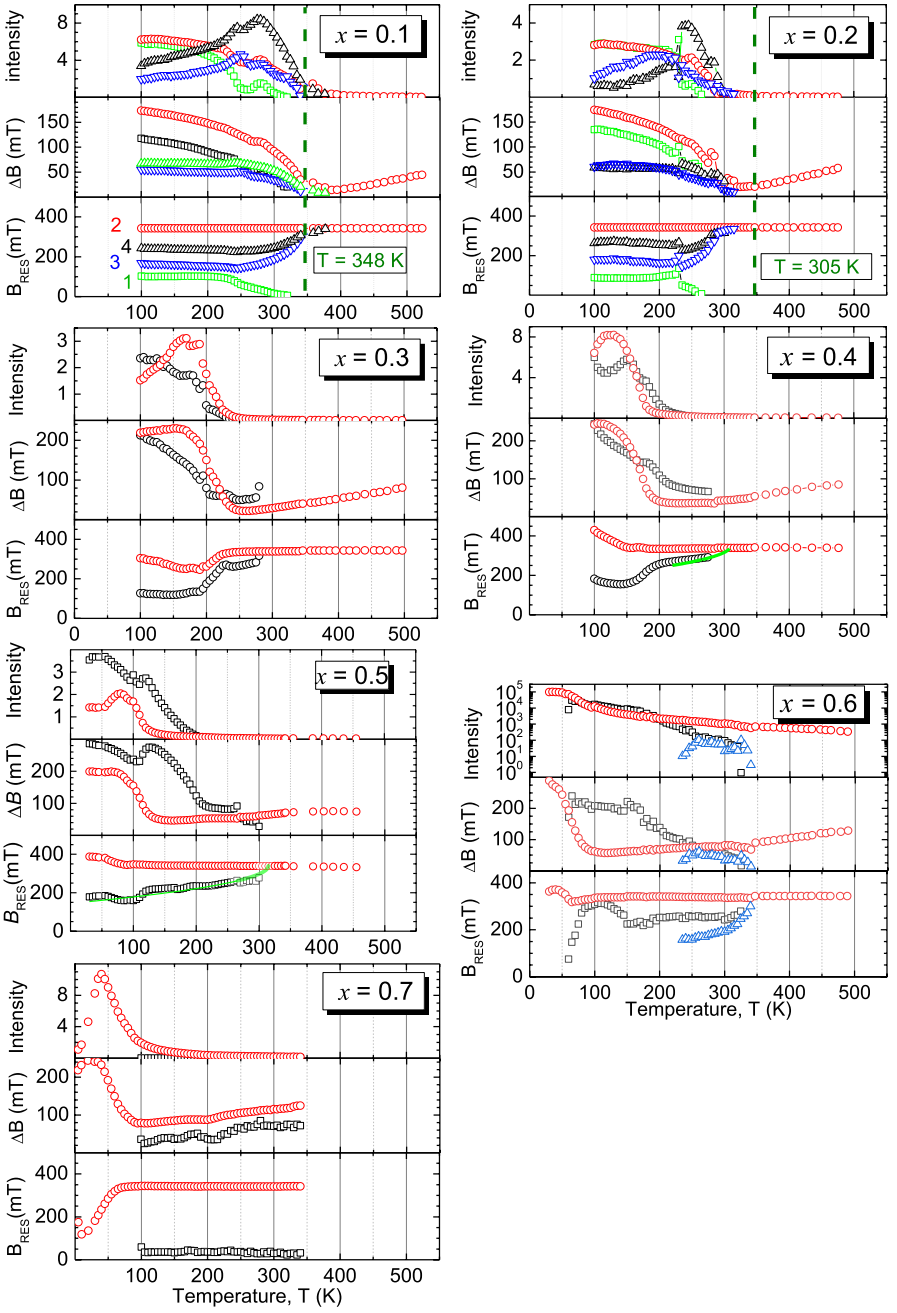


**Fig. 4** Temperature variations of the resonant field $B_{RES}$, line width $\Delta B$ and intensity $I$ of the various components of the EPR spectra of the samples $La_{0.7-x}Eu_xSr_{0.3}MnO_3$ ($x = 0.1$–$0.7$) for lines 1 and 2, and line 3 (when observed)

**Table 1** Ferromagnetic phase transition temperatures $T_C$, $T_{C2}$ and $T_G$ for $La_{0.7-x}Eu_xSr_{0.3}MnO_3$

| $x$ (Eu concentration) | $\theta_{CW}$ (K), this work | $T_C$ (K), this work | $T_C$ (K), [18] | $T_{C2}$ (K), this work (second EPR line) | $T_G$ (K) |
|---|---|---|---|---|---|
| 0.0 | | | 357 | | |
| 0.1 | 387 | 318 | 342 | 255 | |
| 0.2 | 303 | 282 | 292 | 235 | |
| 0.3 | 298 | 195 | 228 | 205 | 295 |
| 0.4 | 216 | 170 | | 170 | 295 |
| 0.5 | 253 | 105 | 111 [35] | 130 | 305 |
| 0.6 | 194 | 55 | | | 305 |
| 0.7 | 97 | 50 | 58 [35] | | |

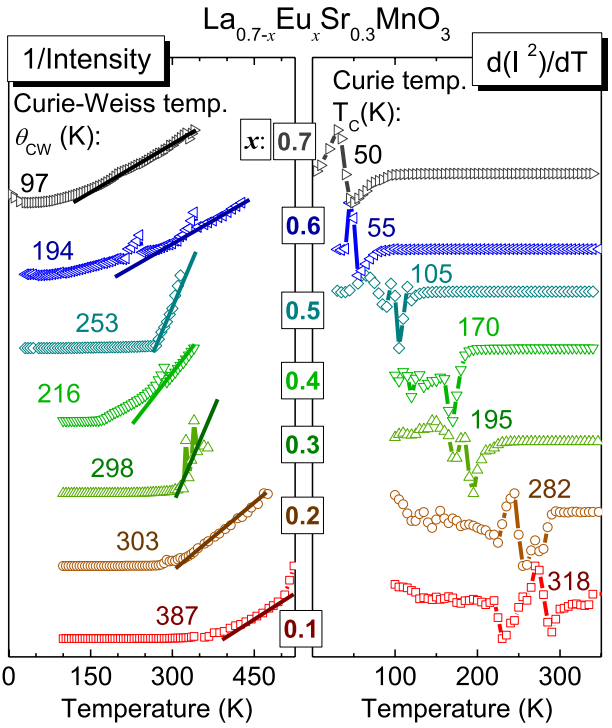


**Fig. 5** Temperature variations of the inverse integral intensity (left part) and those of the first derivatives of the squares of the integral intensity (right part) for the samples $La_{0.7-x}Eu_xSr_{0.3}MnO_3$ ($x = 0.1$, 0.2, 0.3, 0.4, 0.5, 0.6, 0.7)

$$1/I\ (T - \theta_{CW})/\text{const} \tag{2}$$

The fitted temperature variations of the first derivative of the square of the integral intensity and that of the inverse integral intensity are shown in Fig. 5 to determine $T_C$ and $\theta_{CW}$, respectively, for the $La_{0.7-x}Eu_xSr_{0.3}MnO_3$ ($x = 0.1$, 0.2, 0.3, 0.4, 0.5, 0.6,

0.7) samples. It is clearly seen from this figure that the phase-transition temperature, $T_C$, decreases with increasing Europium concentration. As for $\theta_{CW}$, considering the error bars, which is about 15% for each $\theta_{CW}$, one can say that the Curie–Weiss temperature, $\theta_{CW}$, also decreases with increasing Europium concentration, within error bars.

#### 2.4.1 $La_{0.6}Eu_{0.1}Sr_{0.3}MnO_3$

The EPR spectrum of the $La_{0.6}Eu_{0.1}Sr_{0.3}MnO_3$ perovskite is shown in Fig. 2. It indicates that the Curie temperature is about 340 K, since below this temperature, a sharp decrease in the resonance field of the ferromagnetic line is observed. In the plot of the temperature dependence of the linewidth $\Delta B$ in Fig. 3a, a uniform broadening of both the ferromagnetic and paramagnetic lines below 340 K is seen. In the temperature range from 240 to 305 K, one more signal is observed, which is denoted as 3. This signal also appears in the EPR spectra for $La_{0.7-x}Eu_xSr_{0.3}MnO_3$ perovskites with the Eu concentrations $x=0.2$ and 0.3. This line is observed only in the temperature interval from $T^*_{2C}$, referred to hereafter as the Curie temperature for line 2, to $T_C$, as seen from Fig. 4. For the samples with $x>0.3$, this line disappears as seen from Fig. 4. Interpretation of line 3 requires further study as this line is unexpected. However, it is noted that, in contrast to the ferromagnetic and paramagnetic signals, whose resonant fields increase with increasing temperature, the resonant field of this unknown signal decreases with increasing temperature, requiring further study.

#### 2.4.2 $La_{0.5}Eu_{0.2}Sr_{0.3}MnO_3$

From the temperature dependence of the EPR spectrum in Fig. 3, it is seen that.

(1) the linewidth begins to increase sharply below 295 K as the temperature decreases, implying that the Curie temperature of this sample is about 295 K.
(2) the resonance fields for the two lines decrease sharply with decreasing temperature, starting from 300 K; and
(3) broadening of these lines is observed below 305 K. This indicates that the ferromagnetic transition occurs at about 300 K. Since the Curie temperature $T_C$ of the perovskite $La_{0.5}Eu_{0.2}Sr_{0.3}MnO_3$ is close to room temperature, it is potentially useful in the design of magnetocaloric refrigeration units as a working fluid.

#### 2.4.3 $La_{0.4}Eu_{0.3}Sr_{0.3}MnO_3$

For this sample, it is observed that the linewidth begins to increase below 230 K as the temperature decreases (Fig. 4). A sharp decrease in the resonant field of this line is observed below 225 K (Fig. 4). In addition, at this temperature, there occurs a sharp broadening of the resonance lines of both the ferromagnetic and paramagnetic signals (Fig. 4). This indicates that the ferromagnetic phase transition temperature for this sample is 225 K. It is also noted that for the sample with the Eu

concentration $x = 0.3$, 0.6 the third line, is still observed at room temperature, but its intensity is very low. On the other hand, this line is absent from the samples with the Eu concentrations of $x = 0.4$–0.5.

#### 2.4.4 $La_{0.3}Eu_{0.4}Sr_{0.3}MnO_3$

For this sample, the unusual third line, as observed in the samples with $x < 0.4$, is no longer observed. Upon examining the temperature variation of the EPR spectra for this sample, it is seen that a significant line broadening occurs around 185 K, as seen in Fig. 4, which also shows that a sharp decrease in the resonant fields for the two observed EPR lines is seen as the temperature is decreased at approximately the same temperature (185 K).

#### 2.4.5 $La_{0.7-x}Eu_xSr_{0.3}MnO_3$ ($x = 0.5$–0.7)

Using the same analysis as described above, the ferromagnetic phase-transition temperatures were determined for the two perovskites $La_{0.2}Eu_{0.5}Sr_{0.3}MnO_3$ and $La_{0.1}Eu_{0.6}Sr_{0.3}MnO_3$to be 110 K, and for $Eu_{0.7}Sr_{0.3}MnO_3$ to be 55 K (Fig. 4). The estimated $T_C$ values for the samples with various Eu concentrations are listed in Table 1. A phase diagram was made, using the data listed in this table, as shown in Fig. 6, displaying the dependence of $T_C$ on the Eu concentration in the $La_{0.7-x}Eu_xSr_{0.3}MnO_3$ perovskites, with $x = 0.1$–0.7. It is noted from this figure that the values $T_C$ for the Eu concentrations $x = 0.1$, 0.2 and 0.3 are in good agreement with the $T_C$ values reported in Ref. [18], where the $T_C$ values were determined by several methods: modified Arrott plots, Kouvel–Fischer technique, and critical isotherms.

It is noted that there are seen some differences in the Curie temperatures as derived from the EPR data and those listed in Ref. 18 for the samples, $x = 0.1$, 0.2 and 0.3. This is because different experimental methods were used in these two cases. Furthermore, although there were observed three phases in each of these samples, the Curie temperatures (shown in Table 1) were obtained from the behavior of only one phase. This accounts for the differences in the two sets of $T_C$ values.

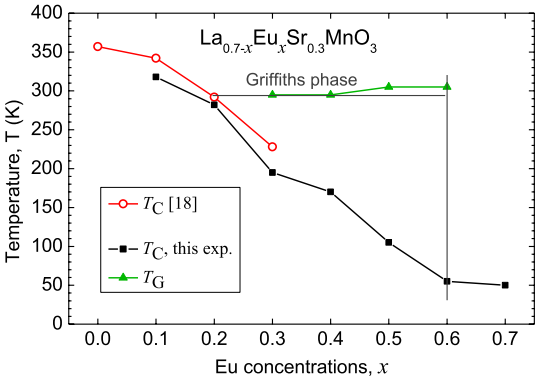


**Fig. 6** Comparison of the ferromagnetic phase transition temperatures, $T_C$, as determined in the present study, with those reported in Ref. [18]. The Griffiths temperatures $T_G$ are deduced from the systematic of the present EPR spectra

### 2.4.6 Dependence of Curie Temperature on the Concentration of Eu

The transition from a paramagnetic insulating to a ferromagnetic metallic state observed in the rare-earth manganites $A_{1-y}B_yMnO_3$ is usually described within the framework of the double-exchange mechanism proposed by Zener [41, 42], where the mobile $3d\ e_g$ electrons of the $Mn^{3+}$ ions couple ferromagnetically to the localized $3d\ t_{2g}$ core spins due to a strong Hund's coupling [43]. Very important parameters in this model, which determine the value of the ferromagnetic phase transition temperature, here are the two Mn–O1–Mn and Mn–O2–Mn bond angles. According to the Double exchange model, the strength of the ferromagnetic interaction decreases with decreasing Mn–O–Mn bond angle, leading to a decrease in its $T_C$. Therefore, a decrease in the Mn–O–Mn bond angle, which occurs as the Eu content increases, leads to a decrease in $T_C$. The tendency to decrease the Mn–O–Mn bond angle is expected to continue for increase in the Eu content for $x > 0.3$ as $x$ increases. Figure 6 and Tables 1 and 2 clearly show that the Curie temperature, $T_C$, decreases with increasing Eu concentration, $x$.

## 2.5 Griffiths Phase

The nature of this phase can be understood in terms of Griffiths singularities arising due to the presence of correlated quenched disorder [44]. From the EPR point of view, the evidence of the formation of Griffiths phase is indicated by the appearance of an additional line, which shifts to low magnetic fields as the temperature decreases below the Curie temperature. In the presence of Griffith phase, the inverse temperature dependence of the magnetic susceptibility deviates from the Curie–Weiss law when measured in low magnetic fields and follows the Curie–Weiss law when measured in strong magnetic fields. In the perovskites $La_{0.7-x}Eu_xSr_{0.3}MnO_3$, with $x = 0.0$–$0.7$, the Griffiths phase appears in the vicinity of 300 K and persists to temperatures as low as 110 K for $x = 0.2$–$0.6$. It indicates the transition to a ferromagnetic phase from the paramagnetic phase as the temperature is lowered, as observed for the resonance line at $g = 2.0$. Griffiths showed that there would develop essential singularities in the temperature region $T_C(p) < T < T_G$. Here $p$ denotes the disorder parameter, $T_C(p)$ is the ferromagnetic ordering temperature,

**Table 2** Mn–O–Mn bond angles [17] and $T_C$ [18]

| Eu content, $x$ | Mn–O1–Mn (°) | Mn–O2–Mn (°) | $T_C$ [18] |
|---|---|---|---|
| 0.0 | 162.26 | | 357 |
| 0.1 | 161.89 | 164.60 | 342 |
| 0.2 | 157.89 | 163.90 | 292 |
| 0.3 | 157.82 | 159.90 | 228 |
| 0.5 | | | 111 [35] |
| 0.7 | | | 58 [35] |

which is disorder-dependent, and $T_G$ is a new temperature scale, which corresponds to $T_C(1)$, the Curie temperature of the undiluted system, which is characterized by $p=1$ [8].

The Griffiths phase temperature $T_G$ was determined here from the temperature dependence of the shift of the resonance field in the Griffiths phase from the resonance field in the paramagnetic phase, $B–B_{res}$ ($L_1$), as described in Ref. [8]:

$$B - B_{res}(L_1) = \text{const} \times \sqrt{1 - T/T_G} \tag{3}$$

The $T_G$ temperatures, as obtained by fitting to Eq. 3 for the various samples, are listed in Table 1. (In Eq. 3, $L_1$ refers to line 1.)

Using the data from Table 1, the $T_C(x)$ phase diagram, as a function of the concentration $x$, was plotted, showing the boundaries of Griffiths phase. Figure 6 shows a phase diagram describing the dependence of the ferromagnetic phase transition temperature on Eu concentration with the demarcation of the boundaries of the Griffiths phase in the perovskites $La_{0.7-x}Eu_xSr_{0.3}MnO_3$, with $x=0.0$–$0.7$. It is concluded from this figure that the Griffiths phase appears in the vicinity of 300 K and persists up to temperatures as low as 110 K for $x=0.2$–$0.6$. As for the samples with $x=0.1$ and $x=0.7$, they do not exhibit any Griffiths phase due to their smaller than the required minimum disorder.

### 2.6 Hopping Conductivity and Estimation of Activation Energy for $La_{0.7-x}Eu_xSr_{0.3}MnO_3$ Samples

Figures 7 and 8 show, respectively, the temperature variations of the linewidths of the EPR lines 1 and 2, observed in the samples $La_{0.7-x}Eu_xSr_{0.3}MnO_3$.

The hopping conductivity of a sample affects significantly its EPR linewidth, $\Delta B_{pp}$ [4, 45, 46]. The dependence of the linewidth on temperature in the paramagnetic region in the $La_{0.7-x}Eu_xSr_{0.3}MnO_3$ samples is almost linear, as seen from Fig. 7. It is due to the small polaron-hopping conductivity as described below by Eq. 4 [9, 10]. The hopping rate limits the lifetime of the charge carriers, e.g.,

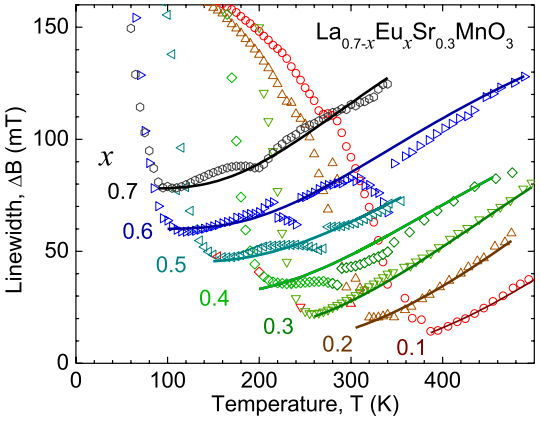


**Fig. 7** Temperature variations of the EPR linewidths of line 1 for the various $La_{0.7-x}Eu_xSr_{0.3}MnO_3$ samples; the corresponding value of $x$ is shown on each plot in the figure

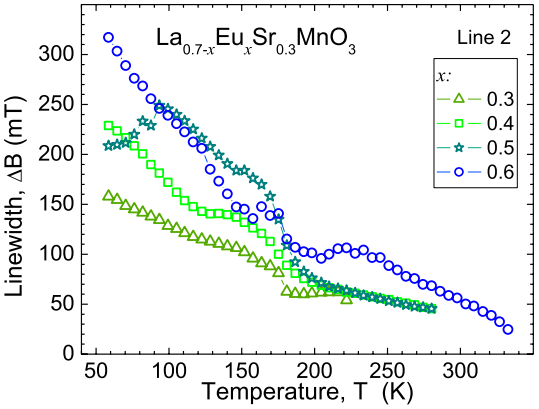


**Fig. 8** Temperature variations of the EPR linewidths of line 2 for the various $La_{0.7-x}Eu_xSr_{0.3}MnO_3$ samples; the corresponding value of $x$ is shown on each plot in the figure

$Mn^{4+}$ spins. In the paramagnetic state, the conductivity varies with the temperature as: $\sigma(T) \propto (1/T) \times \exp(-E_\sigma/k_B T)$ due to the hopping motion of small polarons caused by the motion of charge carriers. Both the EPR linewidth and conductivity increase in proportion to the hopping rate. In the bottlenecked spin-relaxation model, the dependence of $\Delta B_{pp}$ upon the temperature above $T_{min}$ in rare-earth manganites can be described, in similarity to the electrical conductivity in rare-earth manganites, by the following expression [4, 45, 46]:

$$\Delta B_{pp}(T) = \Delta B_{pp\,min} + \frac{A}{T}\exp\left(-\frac{E_a}{k_B T}\right), \tag{4}$$

where $E_a$ is the activation energy for $T > T_{min}$, and $T_{min}$ is the temperature at which the minimum of the EPR linewidth ($\Delta B_{pp\,min}$) is observed. The best-fit parameters for the activation energy, $E_a$, for these samples, as determined by applying the hopping model, where in one fits the EPR linewidth to Eq. 4, were here estimated. The dependence of the fitted values of $E_a$ on the Eu content is shown in Fig. 9. It is seen from this figure that the activation energy, $E_a$, varies almost linearly for samples with

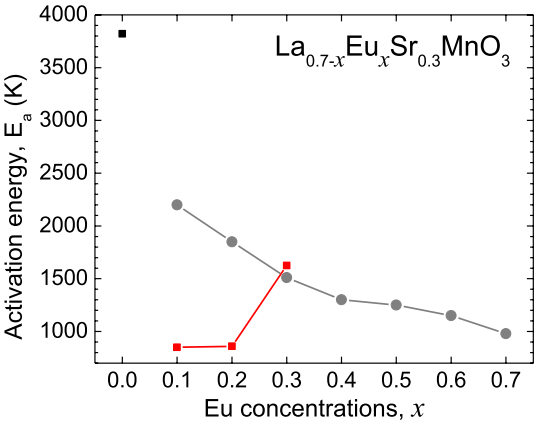


**Fig. 9** The dependence of the activation energy, $E_a$, on the Eu content, $x$. for the samples $La_{0.7-x}Eu_xSr_{0.3}MnO_3$. The black circles represent $E_a$ as estimated by fitting to Eq. 4, with an error of 5–10%, from the temperature dependence of the EPR linewidth in the present work. The red squares represent $E_a$ values derived from the polaron-hopping conductivity data [17]. The value for $E_a$ for the sample with $x = 0.0$ is taken from Ref. [14]

$x = 0.1$–$0.7$ on the concentration of Eu ions, within an error of about 5–10%. The variations of the EPR linewidth with temperature of line 1 for the various samples are shown in Fig. 7. The activation energy $E_a$ for $La_{0.7-x}Eu_xSr_{0.3}MnO_3$ samples with $x = 0.4, 0.5, 0.6, 0.7$, as reported previously in [35], are very close to those obtained in the present work. The $E_a$ values for the samples with $x = 0.1, 0.2, 0.3$ were estimated from the linear part of the temperature variations of the EPR linewidths in the high temperature region $T > 300$ K, as shown in Fig. 7 for line 1. It is also noted that $E_a$ for the sample with $x = 0.0$ was estimated to be 0.33 eV (3820 K) from the temperature dependence of the EPR linewidth [14], included in Fig. 9, which also shows the $E_a$ values derived from the polaron-hopping conductivity [17] for the samples with $x = 0.1, 0.2, 0.3$. It is noted that whereas the values obtained for the sample with $x = 0.3$, as obtained from the two models, agree with each other within error bars, those for the samples with $x = 0.1, 0.2$ show vast differences. In any case, our values show a continuous variation with the concentration, $x$, as one would expect, unlike those obtained from the polaron-hopping conductivity data.

It is noted that the activation energy as obtained here from the linewidth analysis differs markedly from that obtained from the temperature dependencies of the resistivity (Fig. 8), because the tunneling that is present in the resistivity between granules does not affect the EPR linewidth.

## 3 Concluding Remarks

The salient features of the EPR study on the family of $La_{0.7-x}Eu_xSr_{0.3}MnO_3$ perovskites presented in this paper are as follows.

1. The present EPR investigations indicate that the activation energies for the $La_{0.7-x}Eu_xSr_{0.3}MnO_3$ samples derived from the dependence of EPR linewidth on temperature, decreases almost linearly with $x$ from $x = 0.0$ to $x = 0.7$.
2. The linewidths exhibit a pseudolinear temperature dependence in the paramagnetic region for the samples $La_{0.7-x}Eu_xSr_{0.3}MnO_3$. This is consistent with the bottlenecked spin-relaxation model, especially for the samples characterized by the smallest disorder ($x = 0.7, 0.6, 0.5$).
3. The EPR studies on Eu-doped $La_{0.7-x}Eu_xSr_{0.3}MnO_3$ samples reveal the coexistence of two ferromagnetic phases in the samples with $x = 0.4, 0.5, 0.6, 0.7$, whereas, in the samples with $x = 0.1, 0.2$ and 0.3, a coexistence of three ferromagnetic phases is found.
4. The Curie temperatures for the manganites $La_{0.7-x}Eu_xSr_{0.3}MnO_3$ have been estimated here from the behavior of their respective ferromagnetic components in their EPR spectra.
5. According to the Double exchange model, as the concentration of the $Eu^{3+}$ ions increases, the strength of the ferromagnetic interaction decreases due to decrease in the Mn–O–Mn bond angle, leading to a decrease in its $T_C$, as shown in Table 1.

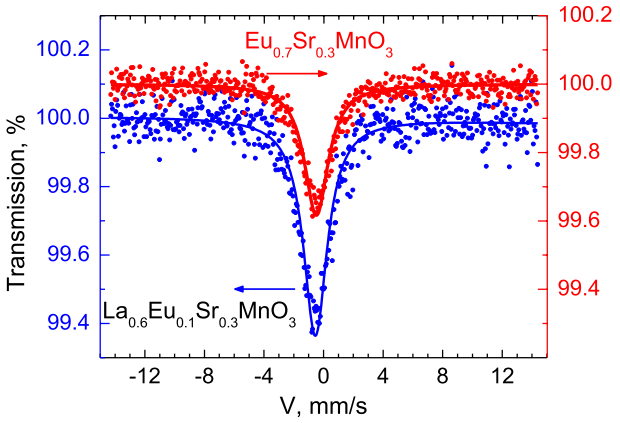


**Fig. 10** Mossbauer spectra of $La_{0.7-x}Eu_xSr_{0.3}MnO_3$, with $x=0.1$ and 0.7, taken at room temperature (295 K) in transmission mode. The spectrum for $Eu_{0.7}Sr_{0.3}MnO_3$ is shifted by 0.1% for clarity of presentation

6. The Griffiths temperatures for the various samples $La_{0.7-x}Eu_xSr_{0.3}MnO_3$ have been estimated here from their respective EPR spectra.
7. The present investigations indicate that the perovskite $La_{0.5}Eu_{0.2}Sr_{0.3}MnO_3$ is potentially useful in the design of magnetocaloric refrigeration units as a working fluid, since its Curie temperature is close to the room temperature.
8. The disordered solid solutions of the manganites $La_{0.7-x}Eu_xSr_{0.3}MnO_3$ are highly inhomogeneous. Their ferromagnetic components have been discerned here by the technique of EPR, not possible by other techniques.

## Appendix: Mossbauer Spectroscopy of $La_{0.6}Eu_{0.1}Sr_{0.3}MnO_3$ and $Eu_{0.7}Sr_{0.3}MnO_3$

It is well known from the isomer-shift data that there is manifested a large separation (more than 10 mm/s) between the compounds containing $Eu^{2+}$ and $Eu^{3+}$ ions. This is due to different shielding of the closed-shell *s*-electrons by the $4^6$ and $4f^5$ configurations [47, 48]. It is well known that the valence of the Europium ion in the manganite $Eu_{1-x}Sr_xMnO_3$ is 3 + [22]. Mössbauer spectroscopy was used in the present work to check the degree of oxidation by the measurement of the isomer shifts of the Eu ion in the manganites with different concentration, $x=0.1$ and 0.7 of the Eu ion. Figure 10 shows typical absorption lines obtained for the samples with $x=0.1$ and 0.7. The spectra were taken in transmission mode at 295 K using a MS-2201 spectrometer with a $^{151}Sm_2O_3$ source of 285 MBq radioactivity. The absorber thickness of the samples was 25 mg × Eu/cm$^2$. The isomer-shift values, $\delta_{\text{eff}}=-0.5\pm0.1$ mm/s and $\delta_{\text{eff}}=-0.4\pm0.1$ mm/s, were determined with respect to the absorber $Eu_2O_3$ at $T=295$ K for the samples $La_{0.6}Eu_{0.1}Sr_{0.3}MnO_3$

and $Eu_{0.7}Sr_{0.3}MnO_3$, respectively. These measured isomer shifts confirm unequivocally the trivalent state of the Europium ion in the samples.

**Acknowledgements** S. Asthana acknowledges financial support by project numbers UGC-DAE (CRS/2021-22/03/553) and SERB (CRG/2020/001509) for fabrication of the samples investigated in this paper. Electron spin resonance measurements were performed with the financial support from the government assignment for FRC Kazan Scientific Center of RAS.

**Author Contributions** IIF, AVS, IVY and DVM made all the EPR measurements reported here. AVP made the Mossbauer measurements reported here. RME, along with SIA, prepared the preliminary version of the manuscript. SA and SV prepared the samples investigated here. All authors helped in the interpretation of the various parts of the data reported here. SKM was responsible for verifying all the interpretations of the data, adding additional information required to enhance the impact of the research presented in the paper, checking the English, and for preparing the final version of the manuscript.

**Funding** This work was partially supported by S. Asthana's project numbers UGC-DAE (CRS/2021-22/03/553) and SERB (CRG/2020/001509).

**Data Availability** No datasets were generated or analysed during the current study. The data that support the findings of this study are available from the corresponding author upon a reasonable request.

## Declarations

**Conflict of Interest** The authors declare no competing interests.

**Consent for Publication** Not applicable.

**Ethics Approval and Consent to Participate** Not applicable.

## References

1. D.L. Huber, D. Laura-Cahuana, M. Tovar, M.T. Causa, Electron spin resonance linewidth, susceptibility, and conductivity in doped manganites. J. Magn. Magn. Mater. **310**(2), e604–e606 (2007). https://doi.org/10.1016/j.jmmm.2006.10.715
2. B.I. Kochelaev, E. Shilova, J. Deisenhofer, H.-A. Krug von Nidda, A. Loidl, A.A. Mukhin, A.M. Balbasov, Phase transitions and spin-relaxation in $La_{0.95}Sr_{0.05}MnO_3$. Mod. Phys. Lett. B **17**(10–12), 59–467 (2003). https://doi.org/10.1142/S0217984903005482
3. S.E. Lofland, P. Kim, P. Dahiroc, S.M. Bhagat, S.D. Tyagi, S.G. Karabashev, D.A. Shulyatev, A.A. Arsenov, Y. Mukovskii, Electron spin resonance measurements in $La_{1-x}Sr_xMnO_3$. Phys. Lett. A **233**(4–6), 476–480 (1997). https://doi.org/10.1016/S0375-9601(97)00490-8
4. A. Shengelaya, G. Zhao, H. Keller, K.A. Muller, B.I. Kochelaev, EPR in $La_{1-x}Ca_xMnO_3$: relaxation and bottleneck. Phys. Rev. B **61**, 5888–5890 (2000). https://doi.org/10.1103/PhysRevB.61.5888
5. C. Rettori, D. Rao, J. Singley, D. Kidwell, S.B. Oseroff, M.T. Causa, J.J. Neumeier, K.J. McClellan, S.-W. Cheong, S. Schultz, Temperature dependence of the EPR linewidth in the paramagnetic phase ($T > T_C$) of $R_{1-x}B_xMnO_{3+\delta}$ (R = La, Pr; B = Ca, Sr). Phys. Rev. B **55**, 3083–3086 (1997). https://doi.org/10.1103/PhysRevB.55.3083
6. M.T. Causa, M. Tovar, A. Caneiro, F. Prado, G. Ihaňez, C.A. Ramos, A. Butera, A. Alascio, X. Obrados, S. Piñol, F. Rivadulla, C. Vázquez-Vázquez, M.A. López-Quintela, J. Rivas, Y. Tokura, S.B. Oseroff, High-temperature spin dynamics in CMR manganites: EPR and magnetization. Phys. Rev. B **58**, 3233–3239 (1998). https://doi.org/10.1103/PhysRevB.58.3233
7. M.T. Causa, G. Alejandro, R. Zysler, F. Prado, A. Caneiro, M. Tovar, Jahn-Teller effects on the superexchange interactions in $LaMnO_3$. J. Magn. Magn. Mater. **196–197**, 506–508 (1999). https://doi.org/10.1016/S0304-8853(98)00856-7

8. J. Deisenhofer, D. Braak, H.-A. Krug von Nidda, J. Hemberger, R.M. Eremina, V.A. Ivanshin, A.M. Balbashov, G. Jug, A. Loidl, T. Kimura, Y. Tokura, Observation of a Griffiths phase in paramagnetic $La_{1-x}Sr_xMnO_3$. Phys. Rev. Lett. **95**(4), 257202 (2005). https://doi.org/10.1103/PhysRevLett.95.257202
9. X.J. Chen, C.L. Zhang, C.C. Almasan, J.S. Gardner, J.L. Sarrao, Small-polaron hopping conduction in bilayer manganite $La_{1.2}Sr_{1.8}Mn_2O_7$. Phys. Rev. B **67**, 094426 (2003). https://doi.org/10.1103/PhysRevB.67.094426
10. G. Zhao, H. Keller, R.L. Greene, K.A. Muller, in *Physics of Manganites*. ed. by T.A. Kaplan, S.D. Mahanti (Plenum, New York, 1999), p.221
11. M. Paraskevopoulos, F. Mayr, J. Hemberger, A. Loidl, R. Heichele, D. Maurer, V. Müller, A.A. Mukhin, A.M. Balbashov, Magnetic properties and the phase diagram of $La_{1-x}Sr_xMnO_3$ for $x \leq 0.2$. J. Phys. Condens. Matter **12**, 3993–4011 (2000). https://doi.org/10.1088/0953-8984/12/17/307
12. V.N. Krivoruchko, A.I. Marchenko, A.A. Prokhorov, Superparamagnetic resonance of single-domain nanoparticles of $LaSrMnO_3$. Low Temp. Phys. **33**, 433–438 (2007). https://doi.org/10.1063/1.2737553
13. A.I. Shames, E. Rozenberg, G. Gorodetsky, A.A. Arsenov, D.A. Shulyatev, Y.M. Mukovskii, A. Gedanken, G. Pang, Electron magnetic resonance studies of magnetic inhomogeneities in crystalline and nanosized powders of $La_{1-x}Sr_xMnO_3$. J. Appl. Phys. **91**, 7929–7931 (2002). https://doi.org/10.1063/1.1446129
14. T.-L. Phan, N.V. Khiem, J. Zidanic, N.X. Phuc, S.-C. Yu, Influence of A-site substitution on the EPR parameters of $La_{0.7}A_{0.3}MnO_3$ (A = Sr, Ba) compounds. IEEE Trans. Magn. **41**, 2769–2771 (2005). https://doi.org/10.1109/TMAG.2012.2202640
15. S. Vadnala, P. Pal, S. Asthana, Investigation of near room temperature magnetocaloric, magnetoresistance and bolometric properties of $Nd_{0.5}La_{0.2}Sr_{0.3}MnO_3$:$Ag_2O$ manganites. J. Mater. Sci. Mater. Electron. **27**, 6156–6165 (2016). https://doi.org/10.1007/s10854-016-4543-0
16. S. Vadnala, P. Pal, S. Asthana, Asthana, Influence of A-site cation disorder on structural and magnetocaloric properties of $Nd_{0.7-x}La_xSr_{0.3}MnO_3$ ($x = 0.0$, 0.1, 0.2 & 0.3). J Rare Earth **33**(10), 1072–1080 (2015). https://doi.org/10.1016/S1002-0721(14)60528-7
17. S. Vadnala, T.D. Rao, P. Pal, S. Asthana, Study of structural effect on Eu-substituted LSMO manganite for high temperature coefficient of resistance. Physica B **448**, 277–280 (2014). https://doi.org/10.1016/j.physb.2014.04.029
18. S. Vadnala, S. Asthana, Magnetocaloric effect and critical field analysis in Eu substituted $La_{0.7-x}Eu_xSr_{0.3}MnO_3$ ($x = 0.0$, 0.1, 0.2, 0.3) manganites. J. Magn. Magn. Mater. **446**, 68–79 (2018). https://doi.org/10.1016/j.jmmm.2017.09.001
19. S.K. Misra, S.I. Andronenko, S. Asthana, D. Bahadur, A variable-temperature EPR study of the manganites $(La_{1/3}Sm_{2/3})_{2/3}Sr_xBa_{0.33-x}MnO_3$ ($x = 0.0$, 0.1, 0.2, 0.33): small polaron hopping conductivity and Griffiths phase. J. Magn. Magn. Mater. **322**, 2902–2907 (2010). https://doi.org/10.1016/j.jmmm.2010.05.003
20. S.I. Andronenko, A.A. Rodionov, A.V. Fedorova, S.K. Misra, Electron paramagnetic resonance study of $(La_{0.33}Sm_{0.67})_{0.67}Sr_{0.33-x}Ba_xMnO_3$ ($x < 0.1$): Griffiths phase. J. Magn. Magn. Mater. **326**, 151–156 (2013). https://doi.org/10.1016/j.jmmm.2012.08.017
21. G. Alejandro, M.C.G. Passeggi, D. Vega, C.A. Ramos, M.T. Causa, M. Tovar, R. Senis, Temperature evolution of crystal field interactions across the Jahn-Teller transition in a $La_{7/8}Sr_{1/8}MnO_3$ single crystal. Phys. Rev. B **68**(15), 214429 (2003). https://doi.org/10.1103/PhysRevB.68.214429
22. R.M. Eremina, I.I. Fazlizhanov, I.V. Yatsyk, K.R. Sharipov, A.V. Pyataev, H.-A. Krug von Nidda, N. Pascher, A. Loidl, K.V. Glazyrin, Y.M. Mukovskii, Phase separation in paramagnetic $Eu_{0.6}La_{0.4-x}Sr_xMnO_3$. Phys. Rev. B **84**(7), 064410 (2011). https://doi.org/10.1103/PhysRevB.84.064410
23. A.N. Ulyanov, D.S. Yang, A.S. Mazur, V.N. Krivoruchko, G.G. Levhenko, I.A. Danilenko, T.E. Konstantinova, Local structure and magnetic inhomogeneity of nano-sized $La_{0.7}Sr_{0.3}MnO_3$ manganites. J. Appl. Phys. **109**, 123928 (2011). https://doi.org/10.1063/1.3603003
24. I. Mansuri, D. Varshney, N. Kaurav, C.L. Lu, Y.K. Kuo, Effects of A-site disorder on magnetic, electrical and thermal properties of $La_{0.5-x}Ln_xCa_{0.5-y}Sr_yMnO_3$ manganites. J. Magn. Magn. Mater. **323**, 316–323 (2011). https://doi.org/10.1016/j.jmmm.2010.09.026
25. S. Angappane, G. Rangarajan, K. Sethupathi, Magnetic clusters in $Nd_{1-x}Sr_xMnO_3$ ($0.3 < x < 0.5$): an electron-spin resonance study. J. Appl. Phys. **98**, 8334–8336 (2003). https://doi.org/10.1063/1.1555316

26. Q. Huang, A. Santoro, J.W. Lynn, R.W. Erwin, J.A. Borchers, J.L. Peng, R.L. Greene, Structure and magnetic order in undoped manganites. Phys. Rev. B **55**, 14987–14999 (1997). https://doi.org/10.1103/PhysRevB.55.14987
27. G.N. Jonker, J.H. van Santen, Ferromagnetic compounds of manganese with perovskite structure. Physica **16**(3), 337–349 (1950). https://doi.org/10.1016/0031-8914(50)90033-4
28. J.M.D. Coey, M. Viret, L. Ranno, K. Ounadjela, Electron localization in mixed-valence manganites. Phys. Rev. Lett. **75**, 3910–3913 (1995). https://doi.org/10.1103/PhysRevLett.75.3910
29. M. Viret, L. Ranno, J.M.D. Coey, Magnetic localization in mixed-valence manganites. Phys. Rev. B **55**, 8067–8070 (1997). https://doi.org/10.1103/PhysRevB.55.8067
30. S.C. Bhargava, S. Singh, D.C. Kundaliyaand, S.K. Malik, Phase separation in $La_{0.67}Ca_{0.33}Mn_{0.9}Fe_{0.1}O_3$: a Mössbauer study. J. Phys: Condes. Matter. **16**, 1665–1678 (2004). https://doi.org/10.1088/0953-8984/16/9/014
31. S.C. Bhargava, H.P. Kunkel, S. Singh, S.K. Malik, D.D. Buddhikot, A.H. Morrish, Phase separations in $La_{0.7-x}Dy_xCa_{0.3}Mn(Fe)O_3$. Phys. Rev. B **71**, 104419 (2005). https://doi.org/10.1103/PhysRevB.71.104419
32. S.C. Bhargava, S. Singh, S.K. Malik, Critical composition of $La_{0.7-x}Dy_xCa_{0.3}Mn(Fe)O_3$ for high CMR. JMMM **311**(2), 594–604 (2007). https://doi.org/10.1016/j.jmmm.2006.08.038
33. S. Vadnala, N.B. Srivastava, S. Asthana, Nature of correlated polaron hopping mechanism in A-site cation disorder $Nd_{0.7-x}La_xSr_{0.3}MnO_3$ ($x = 0.0$, 0.1, 0.2 and 0.3) manganites. Appl. Phys. A **126**, 155 (2020). https://doi.org/10.1007/s00339-020-3333-y
34. B. Pan, X. Luo, J. Fang, Q. Wu, N. Yu, Y. Yu, M. Pan, H. Yang, H. Ge, Structural, magnetic and magnetocaloric investigation of $La_{0.7-x}Eu_xBa_{0.3}MnO_3$ manganites. Bull. Mater. Sci. **46**, 59 (2023). https://doi.org/10.1007/s12034-022-02882-3
35. S.K. Misra, S.I. Andronenko, P. Padia, S. Vadnala, S. Asthana, EPR and magnetization studies of the manganites $La_{0.7-x}Eu_xSr_{0.3}MnO_3$ ($x = 0.4$, 0.5, 0.6, 0.7) and $La_{0.3}Nd_{0.4}Sr_{0.3}MnO_3$ at different temperatures: conductivity due to hopping of small polarons. J. Magn. Magn. Mater. **519**, 167450 (2021). https://doi.org/10.1016/j.jmmm.2020.167450
36. Y. Tokura, Y. Tomioka, Colossal magnetoresistive manganites. J. Magn. Magn. Mater. **200**(1–3), 1–23 (1999). https://doi.org/10.1016/S0304-8853(99)00352-2
37. M.H. Phan, S.C. Yu, Review of the magnetocaloric effect in manganite materials. J. Magn. Magn. Mater. **308**(2), 325–340 (2007). https://doi.org/10.1016/j.jmmm.2006.07.025
38. J.M.D. Coey, M. Viret, S. von Molnár, Mixed-valence manganites. Adv. Phys. **48**(2), 167–293 (1999). https://doi.org/10.1080/000187399243455
39. N. Paul, S. Vadnala, S. Bonam, A. Agrawal, S.R.K. Vanjari, S.G. Singh, Fabrication and characterization of suspended $La_{0.7}Sr_{0.3}MnO_3$ nanofibers for high-sensitive and fast-responsive infrared bolometer. J. Micromech. Microeng. **33**, 125008 (2023). https://doi.org/10.1088/1361-6439/ad0a3c
40. C.C. Oliva, F. Orsini, S. Cappelli, P. Arosio, M. Allieta, M. Coduri, M. Scavini, Electron spin resonance and atomic force microscopy study on gadolinium doped. J. Spectrosc. **2015**, 491840 (2017). https://doi.org/10.1155/2015/491840
41. C. Zener, Interaction between the *d*-shells in the transition metals. II. Ferromagnetic compounds of manganese with perovskite structure. Phys. Rev. **82**, 403–405 (1951). https://doi.org/10.1103/PhysRev.82.403
42. P.W. Anderson, H. Hasegawa, Considerations on double exchange. Phys. Rev. **100**, 675–680 (1955). https://doi.org/10.1103/PhysRev.100.675
43. P.G. de Gennes, Effects of double exchange in magnetic crystals. Phys. Rev. **118**, 141–153 (1960). https://doi.org/10.1103/PhysRev.118.141
44. R.B. Griffiths, Nonanalytic behavior above the critical point in a random ising ferromagnet. Phys. Rev. Lett. **23**, 17–19 (1969). https://doi.org/10.1103/PhysRevLett.23.17
45. A. Shengelaya, G. Zhao, H. Keller, K.A. Müller, EPR evidence of Jahn–Teller polaron formation in $La_{1-x}Ca_xMnO_{3-y}$. Phys. Rev. Lett. **77**, 5296–5299 (1996). https://doi.org/10.1103/PhysRevLett.77.5296
46. A. Shengelaya, G. Zhao, H. Keller, K.A. Müller, EPR evidence for Jahn–Teller polarons in $La_{1-x}Ca_xMnO_{3+y}$. Phys. C: Supercond. **282–287**, 190–193 (1997). https://doi.org/10.1016/S0921-4534(97)00192-5
47. N.N. Greenwood, T.C. Gibb, *Mössbauer Spectroscopy* (Chapman and Hall Ltd, London, 1971), pp.1–659

48. V.K. Sharma, G. Klingelhofer, T. Nishida (eds.), *Mössbauer Spectroscopy: Applications in Chemistry, Biology, and Nanotechnology* (Wiley, Hoboken, 2013), pp.1–672
49. S.V. Demishev, A.V. Shestakov, I.V. Yatsyk, A.V. Semeno, S.V. Grigoriev, R.M. Eremina, Electron paramagnetic resonance probing of the spin fluctuation transition in the conical spiral phase of MnSi. Solid State Comm. **385**, 115501 (2024). https://doi.org/10.1016/j.ssc.2024.115501



## Authors and Affiliations

**I. Yatsyk[1] · D. V. Mamedov[1] · A. V. Shestakov[2] · I. I. Fazlizhanov[1] · R. M. Eremina[1] · S. I. Andronenko[3] · A. V. Pyataev[3] · S. Vadnala[4] · S. Asthana[5] · S. K. Misra[6]**

✉ S. K. Misra
sushil.misra@concordia.ca

[1] Zavoisky Physical-Technical Institute, FRC Kazan Scientific Center of RAS, Kazan, Russian Federation 420029

[2] Prokhorov General Physics Institute of the Russian Academy of Sciences, Moscow, Russian Federation 119991

[3] Institute of Physics, Kazan Federal University, Kazan, Russian Federation 420008

[4] Department of Physics, School of Advanced Sciences, VIT-AP University, Inavolu, Beside AP Secretariat, Amaravati, Andhra Pradesh 522237, India

[5] Advanced Functional Materials Lab, Physics Department, Indian Institute of Technology, Hyderabad, Telangana 502284, India

[6] Physics Department, Concordia University, 7420 Sherbrooke St. West, Montreal, QC H4B 1R6, Canada